Nanoscale

Accepted Manuscript

This article can be cited before page numbers have been issued, to do this please use: M. Sun, F. Liu, Y. Zhu, W. Wang, J. Hu, J. Liu, Z. Dai, K. Wang, Y. Wei, J. Bai and W. Gao, *Nanoscale*, 2016, DOI: 10.1039/C6NR00056H.

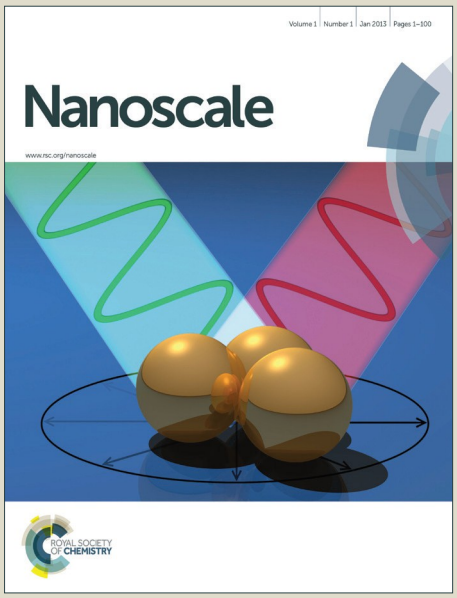

ROYAL SOCIETY OF CHEMISTRY

www.rsc.org/nanoscale

View Article Online
DOI: 10.1039/C6NR00056H

Nanoscale

COMMUNICATION

Salt-Induced Aggregation of Gold Nanoparticles for Photoacoustic Imaging and Photothermal Therapy of Cancer

Received 00th January 20xx,
Accepted 00th January 20xx

DOI: 10.1039/x0xx00000x

www.rsc.org/

Mengmeng Sun,[a] Fei Liu,[a] Yukun Zhu,[b] Wansheng Wang,[a] Jin Hu,[a] Jing Liu,[a] Zhifei Dai,[c] Kun Wang,[b] Yen Wei,[d] Jing Bai[a] and Weiping Gao*[a]

The challenge in photothermal therapy (PTT) is developing biocompatible photothermal transducers that can absorb and convert near-infrared (NIR) light into heat with high efficiency. Herein, we report salt-induced aggregation of gold nanoparticles (GNPs) in biological media to form highly efficient and biocompatible NIR photothermal transducers for PTT and photothermal/photoacoustic (PT/PA) imaging of cancer. The GNP depots *in situ* formed by salt-induced aggregation of GNPs show strong NIR absorption induced by plasmonic coupling between adjacent GNPs and very high photothermal conversion efficiency (52%), enabling photothermal destruction of tumor cells. More interestingly, GNPs *in situ* aggregate in tumors to form GNP depots, enabling simultaneous PT/PA imaging and PTT of the tumors. These findings may provide a simple and effective way to develop a new class of intelligent and biocompatible NIR photothermal transducers with high efficiency for PT/PA imaging and PTT.

Photothermal therapy (PTT), also known as photothermal ablation or optical hyperthermia, has attracted much attention due to its high selectivity to diseased sites and minimal invasiveness to normal tissues.[1-3] PTT is based on localized heating by light absorption for selective destruction of abnormal cells. Near-infrared (NIR) light is generally preferred for PTT, as it can penetrate soft tissues deeply due to the relatively low absorption/scattering by hemoglobin and water in the biological transparent window (650-900 nm).[4] The key component of PTT is photothermal transducers that can absorb and convert NIR light into heat with high efficiency.[1,5]

In the past decades, a variety of NIR photothermal transducers have been developed, including organic compounds (e.g., indocyanine green[6] and porphyrin[7]) or polymers (e.g., polyaniline[8] and polypyrrole[9,10]), metal nanostructures (e.g., gold nanostructures[1,5] and palladium nanoplates[11]), carbon materials (e.g., carbon nanotubes[12] and graphene oxide[13]), copper sulfide nanoparticles[14], tungsten oxide nanowires[15], transition-metal dichalcogenide nanosheets (e.g., molybdenum disulfide[16], tungsten disulfide[17] and bismuth selenide[18]). Of these photothermal transducers, gold nanostructures have been actively studied considering that their localized surface plasmon resonance (LSPR) peaks are located in the NIR region, and gold is inert, biocompatible, non-cytotoxic with a long history of medical use. To date, a variety of gold nanostructures, such as nanoshells[1], nanorods[2], nanostars[19] and nanocages[20] and aggregates of nanoparticles[21-25], have been demonstrated for photothermal cancer therapy with NIR light. However, they are relatively difficult to synthesize and may suffer from chemical contaminations from surfactants such as cetyltrimethylammonium bromide (CTAB)[26] and polymers such as polyethylenimine (PEI)[23] and polystyrene (PS)[24]. These surfactants and polymers are typically cytotoxic. Currently, synthesis of gold nanoparticle (GNP) aggregates requires complicated surface modifications of GNPs with functional compounds such as pH-responsive molecules[21,22] or functional polymers such as amphiphilic block copolymers and self-assembling polymers[23-25]. Furthermore, the photothermal conversion efficiency of these NIR photothermal transducers is low, typically less than 40%[25], which may limit the practical applications of photothermal therapy. Therefore, it is important to develop a simple and effective methodology to form GNP aggregates as highly efficient NIR photothermal transducers.

Department of Biomedical Engineering, School of Medicine, Tsinghua University, Beijing 100084, China. E-mail: gaoweiping@tsinghua.edu.cn
Key Laboratory of Molecular Imaging, the State Key Laboratory of Management and Control for Complex Systems, Institute of Automation, Chinese Academy of Sciences, Beijing, 100190, China.
College of Engineering and Peking University Third Hospital, Peking University, Beijing 100871, China
Department of Chemistry, Tsinghua University, Beijing, 100084, China

†Electronic Supplementary Information (ESI) available: [The experimental strategy of synthesis and characterization of gold nanoparticles, photothermal experiments *in vitro*, photothermal imaging and photoacoustic imaging of tumors, photothermal therapy studies can be found in supporting information. The hydrodynamic radii of gold nanoparticels in different solutions is shown in Table S1. The supplementary data of digital pictures and absorption curves of PEG-GNPs dispersed in different solutions, TEM analyses of tumor injected with PEG-GNPs, more heating curves and photothermal efficiency of GNP depots, photoacoustic signals of GNP depots in tumors, and the change of mouse body weight after PTT are shown in Figure S1-S9.]. See DOI: 10.1039/x0xx00000x

View Article Online
DOI: 10.1039/C6NR00056H

As is well known, high concentration of salts in aqueous solutions can decrease the screening length of charged chemical groups on the nanoparticle surface, consequently inducing the instantaneous and irreversible aggregation of the nanoparticles into large structures that may sediment out of solution as a precipitate (Figure 1A).[27,28] Nevertheless, to our surprise, the salt-induced aggregation of nanoparticles has not been applied as a simple and effective means to develop highly efficient NIR photothermal transducers.

Herein, we report a new class of intelligent and biocompatible NIR photothermal transducers with high efficiency for cancer imaging and photothermal therapy, which are based on salt-induced GNP aggregation. We demonstrate that GNPs that are negatively charged with citrate aggregate in different kinds of biological media, due to salt-induced aggregation of GNPs (Figure 1A), to form GNP depots with strong NIR absorption induced by plasmon coupling effect between adjacent GNPs and very high photothermal conversion efficiency (52%). We show photothermal cancer cell destruction enabled by *in situ* aggregation of GNPs in cell culture media. Furthermore, we demonstrate that GNPs form GNP depots in tumors upon intratumoral injection, enabling simultaneous photothermal/photoacoustic (PT/PA) imaging and photothermal destruction of the tumors (Figure 1B).

Aggregation of GNPs in Biological Media

We observed aggregation of GNPs in ionized aqueous solutions of phosphate buffer saline (PBS), cell culture media and tumor interstitial fluid, as evidenced by instantaneous color changes from red to purple or dark blue (Figure 1C). Dynamic light scattering (DLS) analysis showed that GNPs were monodisperse in deionized aqueous solutions of pure water and 5% glucose with hydrodynamic radii of 9.9 and 11.6 nm, respectively, but became aggregates with significantly increased hydrodynamic radii in these biological media (Figure 1D and Table S1). Transmission electron microscopy (TEM) analysis further confirmed the aggregation of GNPs in PBS, cell culture media and tumor interstitial fluid (Figure 1E). Poly(ethylene glycol) (PEG) is often used to modify GNPs to form PEG-GNPs with improved stability for biomedical applications.[29] As expected, no aggregation was observed for PEG-GNPs in these biological media (Figure S1 and Table S1). Analysis of the UV-vis absorbance spectra revealed that the LSPR peak of GNPs red-shifted to and broadened in the NIR region when the solvent was exchanged from 5% glucose solution to PBS, cell culture media and tumor interstitial fluid (Figure 1F), which is characteristic of the interparticle plasmonic coupling effect[30]. In contrast, no significant red-shift in the LSPR peak was observed for PEG-GNPs (Figure S2), as expected[29]. These results indicate that GNPs aggregate in biological media due to the salt-induced nanocrystal aggregation phenomenon.[27,28]

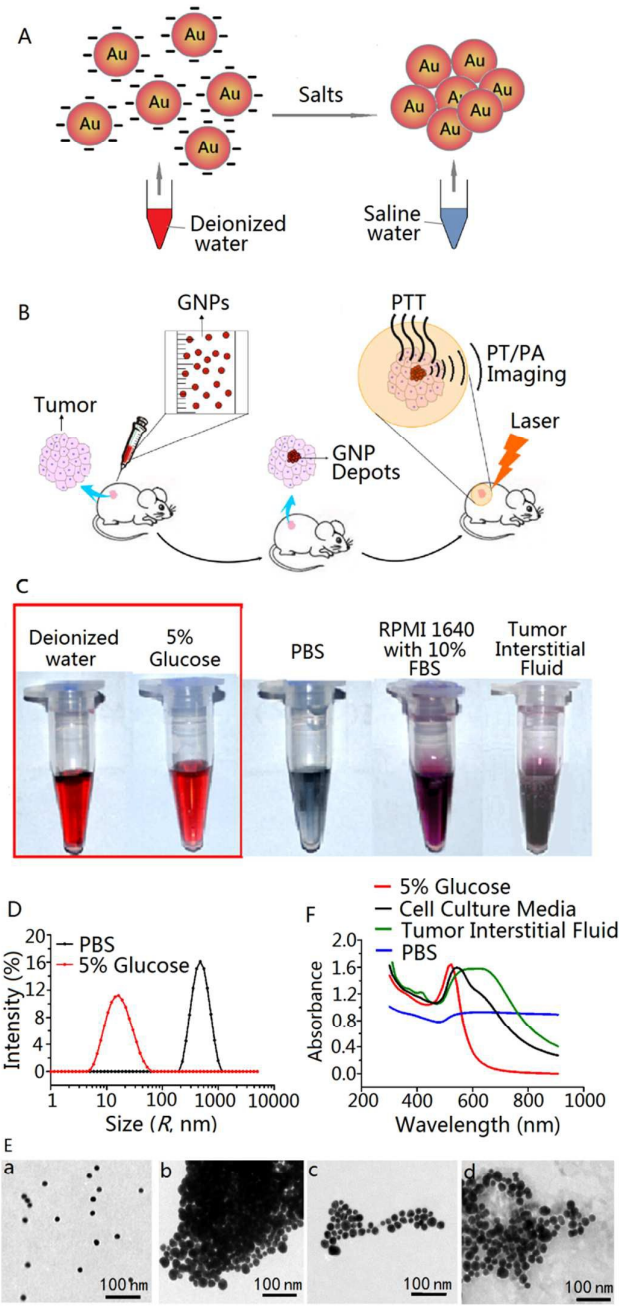

Fig. 1 Aggregation of GNPs in biological media. (A) Schematic illustration of salt-induced aggregation of GNPs that are negatively charged with citrate. (B) Schematic representation of intratumoral aggregation of GNPs to form GNP depots with an ultrastrong plasmonic coupling effect for photoacoustic (PA) imaging, photothermal (PT) imaging and photothermal therapy (PTT) of cancer. (C) Photographs of GNPs dispersed in different biological media. (D) DLS profiles of GNPs in 5% glucose and PBS. (E) TEM images of GNPs in 5% glucose (a), PBS (b), cell culture media (c) and tumor interstitial fluid (d). (F) UV-vis-NIR spectra of GNPs dispersed in different biological media.

View Article Online
DOI: 10.1039/C6NR00056H

Photothermal Effect of GNPs

Motivated by these findings, we hypothesized that GNP depots *in situ* formed by aggregation of GNPs in biological media could be used as highly efficient NIR photothermal transducers. To test the hypothesis, we studied the heating behavior of GNPs in PBS. Upon 808 nm laser irradiation for 5 min, no obvious temperature change was observed in the control of PBS. In contrast, GNPs raised the temperature by 26.3 °C, which is much higher than that (7.1 °C) of PEG-GNPs (Figure 2A). The photothermal effect of GNPs increased monotonically with gold concentration and laser power density, but decreased with incubation time in PBS (Figures S3-S5). These results indicate that GNPs in PBS are more efficient in photothermal effect than PEG-GNPs.

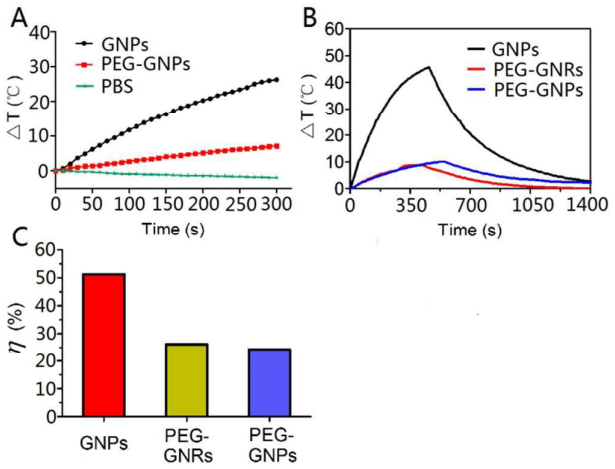

Fig. 2 Photothermal effect of GNPs in PBS. (A) Heating curves of GNPs and PEG-GNPs in PBS at the same gold concentration of 186 μg/mL under the same 808 nm laser power density of 1.5 W/cm^2. (B) Temperature elevation (ΔT) of GNPs, PEG-GNRs and PEG-GNPs in PBS at the same gold concentration of 186 μg/mL exposed to 808 nm laser irradiation (1.5 W/cm^2) as a function of irradiation time. (C) Photothermal conversion efficiencies (η) of GNPs, PEG-GNRs and PEG-GNPs in PBS, which are based on Panel B.

We further measured the photothermal conversion efficiency (η) of GNPs, PEG-GNPs, and PEGylated gold nanorods (PEG-GNRs) as a standard sample according to the well-established method previously reported in the literature[31] (Figure 2B and Figure S6). The η value of GNPs was determined to be 52%, which is 2.2- and 2-fold higher than those of PEG-GNPs (24%) and PEG-GNRs (26%), respectively (Figure 2C). Furthermore, the η value of GNPs is markedly higher than those for gold nanorods (22%), gold nanoshell (13%), gold vesicles (18%), and gold nanovesicles (37%) that were previously reported in the literature[25,31], suggesting very high efficiency of GNPs in PBS in the conversion of the 808 nm laser energy into heat due to the presence of an ultrastrong plasmon coupling effect[25,30].

Photothermal Therapy of Cancer Cells

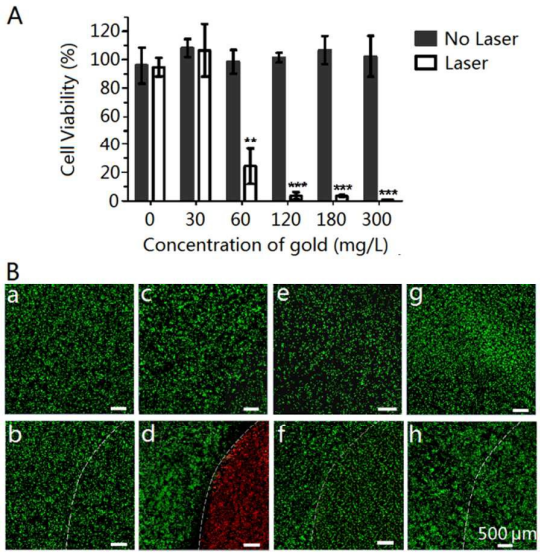

Fig. 3 Photothermal cytotoxicity of GNPs against C26 cancer cells in cell culture media. (A) Cell viability as measured by MTT assay. Data are shown as mean ± SD, n = 3; ** *P* < 0.01 and * *P* < 0.001 for laser irradiation versus no laser irradiation. (B) Confocal fluorescence images of Calcein AM (green)/PI (red) co-stained C26 cells after different treatments at the same gold dose of 186 μg/mL. (a,b) 1640 medium with and without laser irradiation, respectively; (c,d) GNPs in medium with and without laser irradiation, respectively; (e,f) PEG-GNRs in medium with and without laser irradiation, respectively. (g,h) PEG-GNPs in medium with and without laser irradiation, respectively. NIR laser irradiation: 808 nm, 3.5 W/cm^2, 5 min.**

Next, we studied *in vitro* photothermal destruction of cancer cells with GNPs that aggregated in cell culture media (Figure 1C and E). The NIR-laser-triggered cell-killing effect of GNPs was assessed by a standard 3-[4,5-dimethylthiazol-2-yl]-2,5-diphenyltetrazolium bromide (MTT) assay (Figure 3A). Without laser irradiation, GNPs exhibited no toxicity to C26 colon carcinoma cells even if the gold concentration reached 300 mg/L (Figure 3A), indicating GNPs are biocompatible as expected. Upon 808 nm laser irradiation for 5 min at a laser power density of 3.5 W/cm^2, GNPs became cytotoxic when the gold concentration was more than 60 mg/L. To further identify cell viability, we co-stained the cells with Calcein AM and Propidium Iodide (PI) to differentiate live (green) and dead (red) cells, respectively (Figure 3B). Cells treated with only laser irradiation or GNPs alone showed only green fluorescence of Calcein AM, suggesting that exposure of cancer cells to either GNPs or NIR irradiation alone did not cause cell death (Figure 3B (b-c)). All cells were killed after the treatment with GNPs in combination with NIR laser irradiation, as indicated by the intense homogeneous red fluorescence (Figure 3B (d)). Meanwhile, we found that all cells within the laser spot were killed, whereas cells outside the region of the

View Article Online
DOI: 10.1039/C6NR00056H

laser spot (without NIR irradiation) displayed green fluorescence. This result indicates that PTT with GNPs is highly selective and localized. In contrast, the treatment with PEG-GNRs plus NIR laser irradiation caused little cell death, as indicated by the sporadic weak red fluorescence (Figure 3B (f)). As expected, the treatment with PEG-GNPs or PEG-GNRs without NIR laser irradiation or PEG-GNPs in combination with NIR laser irradiation caused no cell death, as indicated by the intense homogeneous green fluorescence (Figure 3B (e,g,h)). These results reveal that GNPs are more efficient NIR photothermal transducers for cancer cell destruction than PEG-GNPs and PEG-GNRs.

Photothermal/Photoacoustic Imaging of Tumors

Encouraged by the *in vitro* PTT effect of GNPs, we further hypothesized that GNPs would *in situ* aggregate in tumors to form GNP depots for *in vivo* PT/PA imaging and PTT. The intratumoral aggregation of GNPs was confirmed by TEM and energy dispersive X-ray spectroscopy (EDS) analyses of the tumor tissue treated with GNPs in a C26 cancer-xenograft model (Figure 4A). GNPs formed irregular aggregates after intratumoral injection, while PEG-GNPs did not aggregate (Figure S7), as expected. Thermal imaging with an infrared thermal camera was used to monitor the *in vivo* photothermal effect (Figure 4B and C). Upon laser irradiation, GNPs rapidly increased the local tumor temperature by more than 29.3 °C within 5 min, and the resulting temperature of 59.2 °C would be high enough to kill tumor cells *in vivo*. No significant temperature increase was observed in other body parts of the mice, indicating that the heating is highly localized. In contrast, PEG-GNRs and PEG-GNPs raised the local tumor temperature by just 20.8 °C and 17.8 °C, respectively, which are just slightly higher than that (15.2 °C) in the case of 5% glucose. Taken together, these results indicate that citrate-GNPs are more effective in photothermal imaging of tumors than PEG-GNPs and PEG-GNRs.

Based on the photothermal imaging results, we further evaluated the PA property of GNPs (Figure 4D). The PA intensity of GNPs was related to the time post injection, which reached a maximal value at 1.5 h post injection (Figure S8), thus providing a non-invasive and *in situ* approach to optimize cancer treatment with GNPs. Intense PA signal (green) was observed in the tumor region injected with GNPs for 1.5 h, while little and no PA signals were observed in the tumor regions injected with PEG-GNRs and PEG-GNPs, respectively. The PA intensity value for GNPs was approximately 1.9- and 4.7-fold stronger than those for PEG-GNRs and PEG-GNPs, respectively (Figure 4E). These results indicate that GNPs are more efficient than PEG-GNRs and PEG-GNPs for cancer PA imaging.

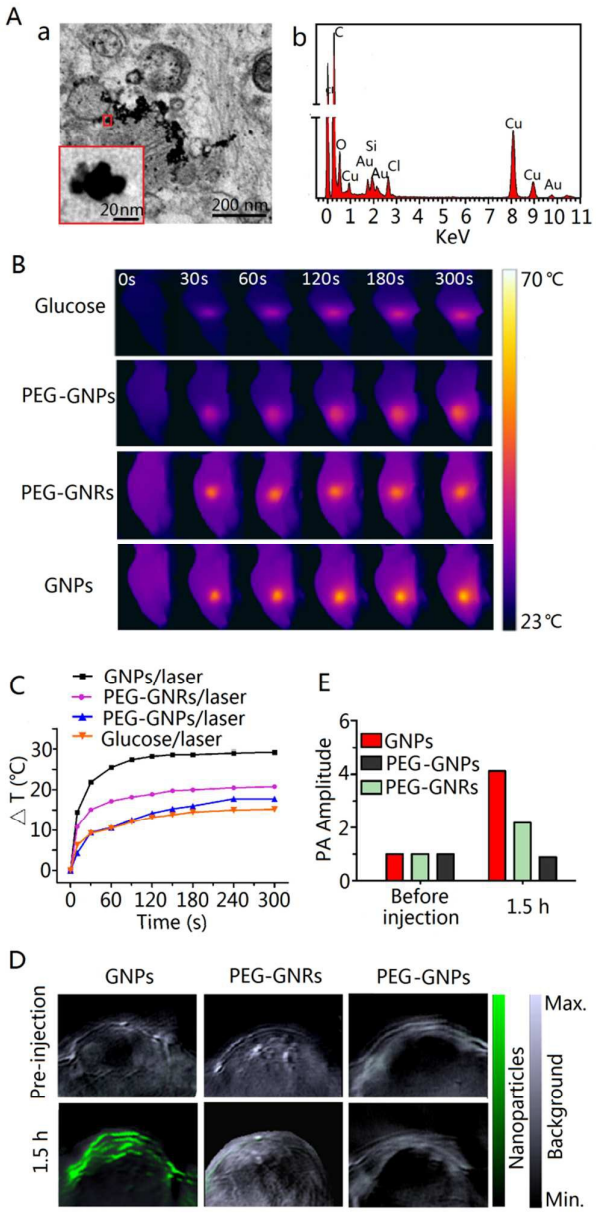

Fig. 4 Photothermal/photoacoustic imaging of tumors post intratumoral injection of GNPs (186 μg/mL, 150 μL). (A) TEM (a) and EDS (b) analyses of tumor tissue containing GNPs in aggregated state. (B) IR thermal images of C26 tumor-bearing mice exposed to an 808 nm laser at a power density of 1.0 W/cm^2 after intratumoral injection with 5% glucose, PEG-GNPs, PEG-GNRs and GNPs. (C) Heat curves of tumors upon laser irradiation as a function of irradiation time. (D,E) PA images and intensities of tumor tissues before and after intratumoral injection of the same gold amount of GNPs, PEG-GNRs and PEG-GNPs for 1.5 h.

View Article Online
DOI: 10.1039/C6NR00056H

Photothermal Therapy of Tumors

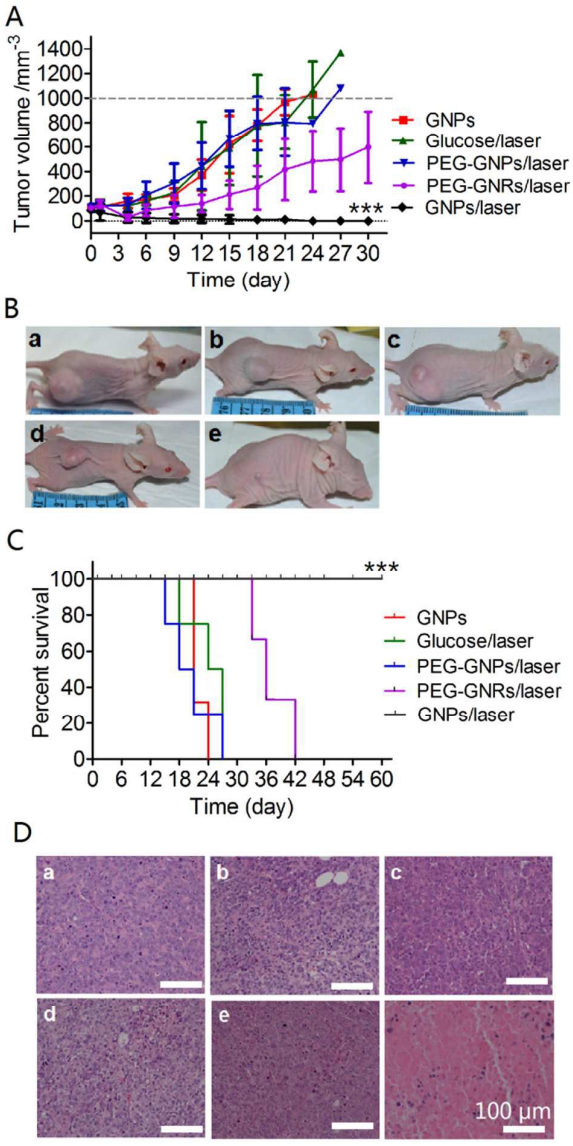

Fig. 5 Photothermal therapy of tumors after intratumoral administration of GNPs (186 μg/mL, 150 μL). (A) Tumor growth curves of different groups of C26 tumor-bearing mice after the treatments. Error bars were based on standard deviations of 3-7 mice per group. (B) Photographs of C26 tumor-bearing mice after the treatments with GNPs (a), PEG-GNPs plus laser (b), 5% glucose plus laser (c), PEG-GNRs plus laser (d), GNPs plus laser (e). (C) Survival curves of mice bearing C26 tumors after various treatments. (D) H&E stained tumor slices collected from different groups of mice immediately after laser irradiation: no treatment (a), laser only (b), 5% glucose plus laser (c), PEG-GNPs plus laser (d), PEG-GNRs plus laser (e) and GNPs plus laser (f). NIR laser irradiation: 808 nm, 1.0 W/cm^2, 5 min. ***P < 0.001, significant difference for GNPs plus laser versus controls.

Guided by these images, we finally studied PTT of tumors at 1.5 h post injection of GNPs (Figure 5). In the group treated with GNPs plus 808 nm laser irradiation at 1.0 W/cm^2 for 5 min, all the tumors were effectively ablated, and black scars were left at the original tumor sites and no recurrence was observed (Figure 5A and B). In contrast, the tumor growth was initially inhibited, but recurrence was observed in the group treated with PEG-GNRs plus 808 nm laser irradiation (Figure 5A and B). As expected, the tumors in the control groups administered with GNPs without laser irradiation, PEG-GNPs with laser irradiation and 5% glucose solution with laser irradiation grew at a similar rate (Figure 5A and B). The mice in the control groups showed average life spans of 15-42 days after the treatments started; in contrast, the mice in the GNPs treated group were tumor-free and survived over 60 days without a single death or tumor recurrence (Figure 5C). Hematoxylin and eosin (H&E) analysis showed significant cancer cell damage in the tumor of the GNPs treated group and moderate cancer cell destruction in the tumor of the PEG-GNR treated group, but not in the other control groups (Figure 5D). No significant body weight loss was observed in different groups after the treatments (Figure S9). Collectively, these results indicate that GNPs are more efficient NIR photothermal transducers for PTT of tumors than PEG-GNPs and PEG-GNRs.

Conclusions

In summary, we for the first time report a simple and effective strategy, based on salt-induced nanocrystal aggregation, to develop a new class of intelligent, biocompatible and highly efficient NIR photothermal transducers for cancer imaging and therapy. Due to salt-induced aggregation, GNPs can aggregate in a variety of biological media to form GNP depots with strong NIR absorption induced by plasmon coupling effect between adjacent GNPs. Notably, GNPs show the highest photothermal conversion efficiency (52%) as compared to gold nanostructures previously reported in the literature[25,31]. In a murine cancer model, GNPs also *in situ* aggregate in tumors to form GNP depots, enabling significantly enhanced PT/PA imaging and PTT efficacy as compared to PEGylated GNPs and GNRs. These findings demonstrate that GNPs are a new class of intelligent NIR photothermal transducers that are of high efficiency in cancer imaging and therapy. Unlike GNP aggregates previously reported in the literature[21-25], GNP depots *in situ* formed by salt-induced aggregation of GNPs do not need complicated surface modifications and are fully biocompatible, thus facilitating their biomedical applications. Considering that PTT is suitable for superficial lesions of skin and luminal organs, we believe that intratumoral administration of GNPs is desirable for PTT.

Acknowledgments

This work was supported by the National Natural Science Foundation of China under Grants No. 21274043, 21534006 and 81227901 and the National Basic Research Program of China (973) under Grant No. 2011CB707701.

View Article Online
DOI: 10.1039/C6NR00056H

References

L. R. Hirsch, R. J. Stafford, J. A. Bankson, S. R. Sershen, B. Rivera, R. E. Price, J. D. Hazle, N. J. Halas, J. L. West, *Proc. Natl. Acad. Sci. USA*, 2003, **100**, 13549.

X. Huang, I. H. El-Sayed, W. Qian, M. A. El-Sayed, *J Am Chem Soc.*, 2006, **128**, 2115.

E. Boisselier, D. Astruc, *Chem Soc Rev.*, 2009, **38**, 1759.

R. Weissleder, *Nat. Biotechnol.*, 2001, **19**, 316.

P. K. Jain, X. Huang, I. H. El-Sayed, M.A. El-Sayed, *Acc. Chem. Res.*, 2008, **41**, 1578.

X. Zheng, F. Zhou, B. Wu, W. R.Chen, D. Xing, *Mol. Pharm.*, 2012, **9**, 514.

J. F. Lovell, C. S. Jin, E. Huynh, H. Jin, C. Kim, J. L. Rubinstein, W. C. W. Chan, W. Cao, L. V. Wang, G. Zheng, *Nat. Mater.*, 2011, **10**, 324.

J. Yang, J. Choi, D. Bang, E. Kim, E. K. Lim, H. Park, J. S. Suh, K. Lee, K. H. Yoo, E. K. Kim, Y. M. Huh, S. Haam, *Angew. Chem. Int. Ed.*, 2011, **50**, 441.

K. Yang, H. Xu, L. Cheng, C. Sun, J. Wang, Z. Liu, *Adv Mater.*, 2012, **24**, 5586.

Z. Zha, X. Yue, Q. Ren, Z. Dai, *Adv. Mater.*, 2013, **25**, 777.

X. Huang, S. Tang, X. Mu, Y. Dai, G. Chen, Z. Zhou, F. Ruan, Z. Yang, N. Zheng, *Nat. Nanotechnol.*, 2011, **6**, 28.

H. K. Moon, S. H. Lee, H. C. Choi, *ACS Nano*, 2009, **3**, 3707.

K. Yang, S. Zhang, G. Zhang, X. Sun, S. T. Lee, Z. Liu, *Nano Lett.*, 2010, **10**, 3318.

M. Zhou, R. Zhang, M. Huang, W. Lu, S. Song, *J. Am. Chem. Soc.*, 2010, **132**, 15351.

Z. Chen, Q. Wang, H. Wang, L. Zhang, G. Song, L. Song, J. Hu, H. Wang, J. Liu, M. Zhu, D. Zhao, *Adv. Mater.*, 2013, **25**, 2095.

S. S. Chou, B. Kaehr, J. Kim, B. M. Foley, M. De, P. E. Hopkins, J. Huang, C. J. Brinker, V. P. Dravid, *Angew. Chem. Int. Ed.,* 2013, **125**, 4254.

L. Cheng, J. Liu, X. Gu, H. Gong, X. Shi, T. Liu, C. Wang, X. Wang, G. Liu, H. Xing, W. B. Bu, B. Sun, Z. Liu, *Adv. Mater.*, 2014, **26**, 1886.

J. Li, F. Jiang, B. Yang, X. R. Song, Y. Liu, H. H. Yang, D. R. Cao, W. R. Shi, G. N. Chen, *Sci. Rep.*, 2013, **3**, 1998.

E. Y. Ye, K. Y. Win, H. R.Tan, M. Lin, C. P. Teng, A. Mlayah, M. Y. Han, *J. Am. Chem. Soc.*, 2011, **133**, 8506.

J. Chen, C. Glaus, R. Laforest, Q. Zhang, M. Yang, M. Gidding, M. J. Welch, Y. Xia, *Small,* 2010, **6**, 811.

J. Nam, N. Won, H. Jin, H. Chung, S. Kim, *J. Am. Chem. Soc.,* 2009, **131**, 13639.

H. Li, X. Liu, N. Huang, K. Ren, Q. Jin, J. Ji, *ACS Appl. Mater. Interfaces.*, 2014, **6**, 18930.

S. Wang, K. J. Chen, T. H. Wu, H. Wang, W. Y. Lin, M. Ohashi, P. Y. Chiou, H. R. Tseng, *Angew. Chem. Int. Ed.*, 2010, **49**, 3777.

J. He, X. Huang, Y. C. Li, Y. Liu, T. Babu, M. A. Aronova; S. Wang, Z. Lu, X. Chen, Z. Nie, *J. Am. Chem. Soc.*, 2013, **135**, 7974.

P. Huang, J. Lin, W. Li, P. Rong, Z. Wang, S. Wang, X. Wang, X. Sun, M. Aronova, G. Niu, R. D. Leapman, Z. Nie, X. Chen, *Angew. Chem. Int. Ed.*, 2013, **52**, 13958.

C. Grabinski, N. Schaeublin, A. Wijaya, H. D'Couto, S. H. Baxamusa, K. Hamad-Schifferli, S. M. Hussain, *ACS Nano.*, 2011, **5**, 2870.

M. Y. Lin, H. M. Lindsay, D. A. Weitz, R. C. Ball, R. Klein, P. Meakin, *Nature*, 1989, **339**, 360.

A. Albanese; W. C. W. Chan, *ACS Nano.*, 2011, **5**, 5478.

D. Kim; S. J. Park, J. H. Lee, Y. Y. Jeong, S. Jon, *J. Am. Chem. Soc.*, 2007, **129**, 7661-7665.

S. K. Ghosh, T. Pal, *Chem. Rev.*, 2007, **107**, 4797.

C. M. Hessel, V. P. Pattani, M. Rasch, M. G. Panthani, B. Koo, J. W. Tunnell, B. A. Korgel, *Nano Lett.*, 2011, **11**, 2560.